



HAL
open science

Understanding VNIR Plagioclase Signatures on Mars Through Petrographic, Geochemical, and Spectral Characterization of Terrestrial Feldspar-Bearing Igneous Rocks

M. Barthez, Jessica Flahaut, Martin Guitreau, G. Ito, R. Pik

► **To cite this version:**

M. Barthez, Jessica Flahaut, Martin Guitreau, G. Ito, R. Pik. Understanding VNIR Plagioclase Signatures on Mars Through Petrographic, Geochemical, and Spectral Characterization of Terrestrial Feldspar-Bearing Igneous Rocks. *Journal of Geophysical Research. Planets*, 2023, 128 (8), 10.1029/2022JE007680 . hal-04176310

HAL Id: hal-04176310

<https://cnrs.hal.science/hal-04176310v1>

Submitted on 12 Aug 2023

HAL is a multi-disciplinary open access archive for the deposit and dissemination of scientific research documents, whether they are published or not. The documents may come from teaching and research institutions in France or abroad, or from public or private research centers.

L'archive ouverte pluridisciplinaire **HAL**, est destinée au dépôt et à la diffusion de documents scientifiques de niveau recherche, publiés ou non, émanant des établissements d'enseignement et de recherche français ou étrangers, des laboratoires publics ou privés.



Distributed under a Creative Commons Attribution - NoDerivatives 4.0 International License

Understanding VNIR Plagioclase Signatures on Mars Through Petrographic, Geochemical, and Spectral Characterization of Terrestrial Feldspar-Bearing Igneous Rocks



Key Points:

- Petrographic and visible near-infrared (VNIR) spectroscopic analyses of both macroscopic samples and powders, of various terrestrial magmatic rocks, are presented
- Feldspar VNIR absorption band (variable position) is visible in the spectra of macroscopic rocks containing 30%–80% of plagioclase
- A range of rock types and compositions could therefore match VNIR feldspar signatures that were recently observed on Mars

Supporting Information:

Supporting Information may be found in the online version of this article.

Correspondence to:




M. Barthez,
marie.barthez@univ-lorraine.fr

Citation:

Barthez, M., Flahaut, J., Guitreau, M., Ito, G., & Pik, R. (2023). Understanding VNIR plagioclase signatures on Mars through petrographic, geochemical, and spectral characterization of terrestrial feldspar-bearing igneous rocks. *Journal of Geophysical Research: Planets*, 128, e2022JE007680. <https://doi.org/10.1029/2022JE007680>

Received 14 NOV 2022

Accepted 12 JUL 2023

M. Barthez¹ , J. Flahaut¹ , M. Guitreau² , G. Ito¹, and R. Pik¹

¹Centre de Recherches Pétrographiques et Géo-chimiques, Université de Lorraine, CNRS UMR-7358, Vandœuvre-lès-Nancy, France, ²Laboratoire Magmas et Volcans, Université Clermont Auvergne, OPGC, CNRS UMR-6524, IRD UMR-163, Clermont-Ferrand, France

Abstract Plagioclase feldspar is a common mineral in terrestrial rocks and has recently been detected on Mars surface with visible near-infrared (VNIR) spectroscopy. The presence of plagioclase using this method is determined through the identification of an absorption band centered around 1.3 μm on reflectance spectra, which requires the incorporation of Fe^{2+} in plagioclase lattice. Previous laboratory studies of powder mixtures showed that plagioclase should only be detectable if present in amounts $>90\%$ as its absorption band can be masked by those of mafic minerals. Plagioclase composition, but also the size of the grains and the associated minerals in a rock, influence the spectral signature of plagioclase feldspars. Thus, the analysis of whole, uncrushed rocks appears to be relevant for comparisons with Mars remote sensing observations that have shown plagioclase-like signatures. In the present work, we performed laboratory measurements on five feldspar-bearing terrestrial rocks of various nature chosen because they reflect the first order terrestrial magmatic variability. The mineralogical composition of these samples, the chemical composition of feldspar crystals, and total rock spectra as well as spectra of each mineral were determined using microscopy, electron microprobe, and VNIR spectroscopy. Our study shows that plagioclase signature is visible on the spectra of macroscopic rocks containing between 30% and 80% plagioclase of different compositions ($\text{An}_{25}\text{-An}_{67}$). Our findings have strong implications for the interpretation of feldspar signatures on Mars, which can belong to a range of feldspar-bearing rocks and could thus provide information about the formation of Mars' crust.

Plain Language Summary Plagioclase feldspar is a common mineral of terrestrial rocks that has recently been detected on the surface of Mars with reflectance spectroscopy. In geology, this method allows to non-quantitatively assess the mineralogical composition of rocks by studying the spectrum of the sunlight reflected by them. Previous laboratory studies of plagioclase powders demonstrated that its spectral signature is quickly masked when mixed with more iron-rich minerals and that 90% plagioclase content may be needed to observe their diagnostic absorption band around 1.3 μm . In the present study, five terrestrial samples of uncrushed rocks of varied nature, which contain plagioclase, were analyzed with instruments for petrographic and spectral characterization. A diverse set of instruments allowed us to obtain the total rock spectrum, its mineralogy, the spectrum of each mineral group, and the chemical composition of plagioclase for each sample. Our results show that plagioclase signature is present in the spectrum of all five rocks despite them having different compositions, textures, and amounts of plagioclase. We further demonstrate that the position of the plagioclase absorption band varies depending on multiple factors. Our findings have strong implications for the interpretation of feldspar signatures on Mars, which could correspond to a range of feldspar-bearing rocks.

1. Introduction

Remote sensing instruments onboard satellites contribute to the understanding of planetary surfaces' geology. Mars remote sensing missions have previously enabled the discovery of water flow features (Fassett & Head, 2005) with Mars Global Surveyor (MGS, Albee et al., 1998), Mars Orbiter Camera (MOC, Malin & Edgett, 2001), MGS Mars Orbiter Laser Altimeter (Zuber et al., 1992), Mars Express (Chicarro et al., 2004) High Resolution Stereo Camera (HRSC, Neukum & Jaumann, 2004), and Mars Odyssey (Saunders et al., 2001) Thermal Emission Imaging System (THEMIS, Christensen et al., 2004), whereas hydrated minerals were detected with the Mars Express Observatoire pour la Minéralogie, l'Eau, les Glaces et l'Activité (OMEGA, Melchiorri et al., 2006) spectral-imaging instrument (Bibring et al., 2006).

© 2023 The Authors.

This is an open access article under the terms of the [Creative Commons Attribution-NonCommercial License](https://creativecommons.org/licenses/by/4.0/), which permits use, distribution and reproduction in any medium, provided the original work is properly cited and is not used for commercial purposes.

More recently, the Mars Reconnaissance Orbiter (MRO, Zurek & Smrekar, 2007) Compact Reconnaissance Imaging Spectrometer for Mars (CRISM, Murchie et al., 2007) detected plagioclase feldspar signatures in the visible-near infrared (VNIR) on the surface of Mars. The detection of such minerals could indicate the presence of a primitive anorthositic crust possibly akin to a magma ocean related flotation crust, as interpreted by Carter and Poulet (2013) and more recently by Phillips et al. (2022). Plagioclase detections could also be accounted for by the volcanic nature of Martian secondary crust (Farrand et al., 2021; Flahaut et al., 2022; Payré et al., 2022; Rogers & Farrand, 2022; Rogers & Nekvasil, 2015) or indicate the presence of felsic rocks such as granodiorites, discovered by the Curiosity rover (Sautter et al., 2015). The detection of plagioclase on Mars surface raises questions regarding the fundamental processes that operated on this planet since the exact origin of these signatures (i.e., the nature of the feldspar-bearing rocks) has sharply distinct implications for our understanding of the formation and evolution of Mars.

Plagioclase feldspar is a common mineral in terrestrial rocks. Its chemical composition varies between two endmembers: sodium-rich albite ($\text{NaAlSi}_3\text{O}_8$), and calcium-rich anorthite ($\text{CaAl}_2\text{Si}_2\text{O}_8$). Plagioclase is most commonly classified based on its anorthite content (An), where albite and anorthite have 0% and 100% An, respectively.

Powders of anorthite-rich plagioclases were previously studied using reflectance spectroscopy in the VNIR range (Adams & Goullaud, 1978). The authors showed that plagioclase feldspar is detectable when it incorporates ferrous iron (Fe^{2+}) in its structure. In this case, an absorption band due to the electronic transitions of iron is visible with band minimum located in the vicinity of 1.3 μm (referred to as the 1.3 μm absorption band) on the reflectance spectrum of plagioclase feldspars. The center of this absorption band and its strength appear to vary with the increase in An content (Adams & Goullaud, 1978), as does the band depth tends to increase with the amount of Fe^{2+} incorporated by plagioclase (Adams & Goullaud, 1978; Bell & Mao, 1973).

Additional laboratory studies carried out on mixtures of binary powders showed that the spectral signature of plagioclase is no longer visible when 10% or more of mafic minerals are added (Cheek & Pieters, 2014; Crown & Pieters, 1987). According to these studies, a minimum of 90% plagioclase feldspar content is necessary in the rock composition for its spectral signature to be distinct on the total rock spectrum. Yet, a different study using a binary mixture of large plagioclase and pyroxene crystals (Rogers & Nekvasil, 2015) showed that up to 50% of mafic minerals could be needed to hide the plagioclase spectral signature.

The key point shown by Rogers and Nekvasil (2015) was that not only the feldspar composition but also the size of the grains (and most likely the associated minerals) in the rock influences the spectral signature and detectability of plagioclase feldspars. Thus, the analysis of whole (uncrushed) rocks appears to be extremely relevant, in addition to previous studies of binary mixtures of powders and grains, for comparisons with Mars remote sensing observations that have shown plagioclase-like signatures (e.g., Carter & Poulet, 2013; Farrand et al., 2021; Flahaut et al., 2022; Payré et al., 2022; Phillips et al., 2022; Rogers & Farrand, 2022; Wray et al., 2013).

The objective of our study is to determine whether plagioclase spectral signature (1.3 μm absorption band), such as those observed on Mars, could be detected in uncrushed terrestrial plagioclase-bearing magmatic rocks ranging from mafic to felsic. To achieve this objective, we measured VNIR reflectance spectra and characterized the petrography of feldspar-bearing rocks using a suite of qualitative and quantitative analytical methods. From these measurements, we investigated the characteristics of the plagioclase absorption band in relation to the chemical composition of plagioclase feldspars and the petrography of their host rock.

Through a repeatable petrographic characterization method, we show that feldspar-like absorption bands are present in all our rock samples containing plagioclase feldspar in varying amounts and compositions. We additionally discuss the possible implications of our findings for the interpretations of Mars hyperspectral observations. The composition of the rocks involved in the detections of feldspar plagioclase on the surface of Mars is still discussed (Carter & Poulet, 2013; Farrand et al., 2021; Flahaut et al., 2022; Payré et al., 2022; Phillips et al., 2022; Rogers & Farrand, 2022; Rogers & Nekvasil, 2015; Sautter et al., 2015). The data collected in our study provide clues to determine the primitive, secondary, or tertiary nature of the rocks involved in these Martian detections.

2. Materials and Methods

Measurements of VNIR reflectance spectra, petrographic and geochemical characterizations were conducted on five macroscopic rock samples. They were chosen because they reflect the first order terrestrial magmatic

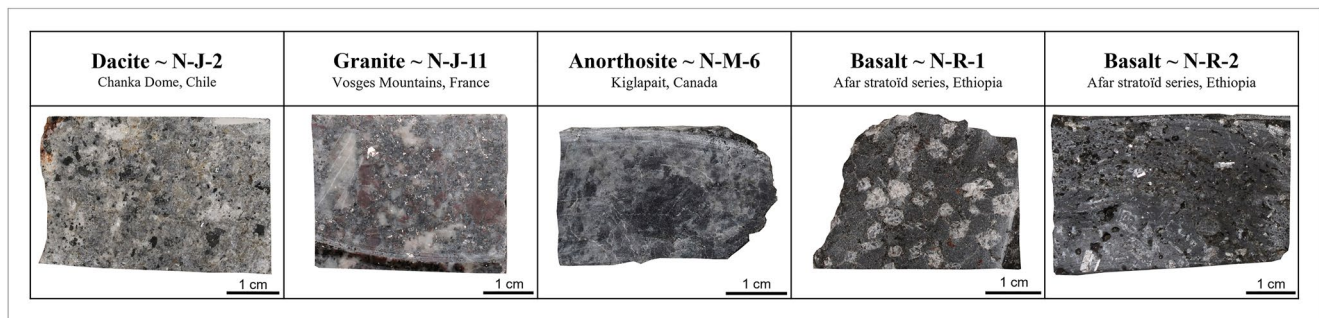


Figure 1. The five macroscopic samples of terrestrial feldspar-bearing rocks cut as regular pieces of about four by three cm. Left to right: dacite NJ2 (Chanka Dome, Chile; De Silva et al., 1994; Flahaut et al., 2021), granite NJ11 (Vosges Mountains, France; Simmler, 1962), anorthosite NM6 (Kiglapait, Canada; Morse, 2015), basalts NR1 and NR2 (Afar, Ethiopia; Pik et al., 1998).

variability from mafic to felsic and from eruptive to plutonic. All samples were cut as shown in Figure 1, and used for both spectral analyses and thin section making.

Terrestrial feldspar-bearing rock samples studied are volcanic or plutonic rocks, from various geographic origins, borrowed from the Centre de Recherches Pétrographiques et Géochimiques (CRPG) researchers' collections:

- NJ2: dacite from Chanka volcanic dome, Atacama Desert, Chile (De Silva et al., 1994; Flahaut et al., 2021);
- NJ11: granite from granitic pluton (« Granite des Crêtes »), Vosges Mountains, France (Simmler, 1962);
- NM6: anorthosite from Kiglapait intrusion, Labrador, Canada (Morse, 2015);
- NR1 and NR2: porphyritic basalts from basaltic flows, Afar triangle, Ethiopia (Pik et al., 1998).

The five rocks were cut homogeneously in the form of sugars of about four by three cm. These samples, NJ2, NJ11, NM6, NR1, and NR2, were studied using six different instruments in order to characterize them spectrally, petrographically, and geochemically. Determining the mineralogical composition of these feldspar-bearing rocks, their reflectance spectrum, and the spectral signature of each mineral in each sample allow us to assess whether the plagioclase feldspar spectral signature contributes significantly to the total rock spectrum of each sample.

2.1. Petrographic and Geochemical Characterization

A petrographic study of each sample was carried out using an optical microscope, as well as geochemical analyses with micro-X-ray fluorescence (μ -XRF) spectroscopy, Scanning Electron Microscope (SEM), and an Electron Probe MicroAnalyzer (EPMA).

The optical microscope uses visible light transmitted through a thin section. The observations were made using both polarized and cross-polarized light.

Micro X-ray fluorescence analyses were performed using a *Bruker M4 Tornado* at GeoRessources, Nancy (France). Under vacuum, an X-ray beam is focused by a polycapillary optics to determine the elemental composition by measuring the energy lost by the atom. The amount of energy lost during the bombing of the sample is unique to each element. Chemical maps of the macroscopic samples were acquired at a resolution of 50 μm per pixel, which included Al, Si, Ca, S, Fe, K, Mg, Mn, Na, Zr, Sr, and Rb (Figure S7 in Supporting Information S1).

Additional chemical maps were acquired using a SEM *JEOL 6510* at CRPG Nancy (France). Thin sections of our samples were coated with carbon prior to analysis. An electron beam obtained by heating a tungsten filament is then focused on the thin section of the sample. The interaction between the incident electrons and the sample causes the formation of lower energy secondary electrons. The microscope detects secondary electrons at each point of the thin section by scanning it. Whole thin sections of the five samples described above were mapped with a resolution of about 1.4 $\mu\text{m}/\text{pixel}$. To obtain this resolution, it was necessary to analyze the thin section in several parts. About 400 images were stitched for each sample using a custom-made Python code to get a global map of the thin sections. The elements analyzed are Al, Si, Ca, S, Fe, K, Mg, Mn, Na, Ni, O, P, Rb, Sr, and Ti. The ENVI image processing software (L3Harris Geospatial) was used to process these chemical maps. By superimposing three chemical maps as red, green, and blue, false color images were created. To highlight the chemical composition diversity of feldspars, false color maps were created with calcium as red, sodium as green,

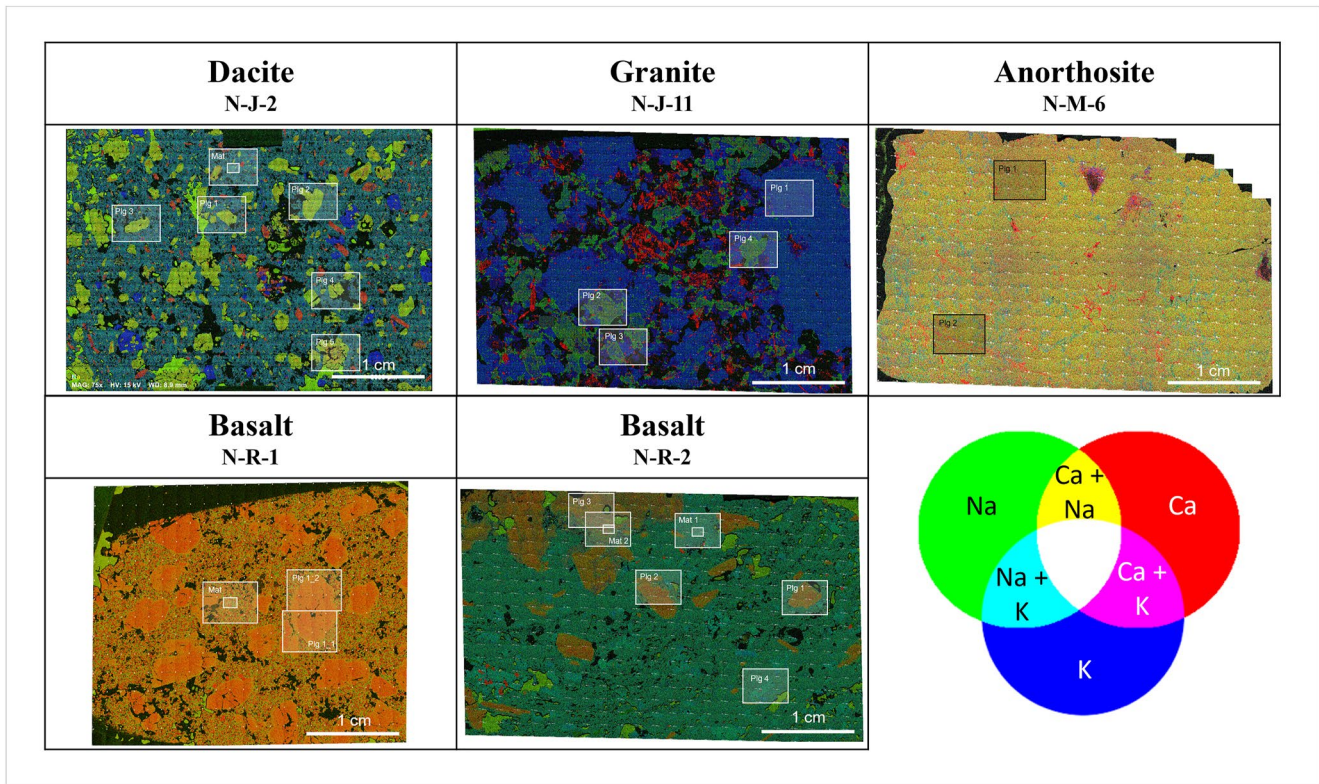


Figure 2. The five feldspar-bearing macroscopic samples NJ2, NJ11, NM6, NR1, and NR2 were analyzed with a Scanning Electron Microscope (SEM). Calcium (Ca), Sodium (Na), and Potassium (K) SEM chemical maps are superimposed as red, green, and blue components, respectively. These false-color maps allow to differentiate calcic, sodic, and potassic feldspars. The Electron Probe MicroAnalyzer (EPMA) analysis points are indicated as white boxes. Both porphyritic and microplitic crystals were targeted with EPMA.

and potassium as blue (Figure 2). One Region Of Interest was created for each mineral contained in each sample to be used as an endmember. Using the Minimum Distance (MD) algorithm, pixels of these images were classified according to their color, and therefore their chemical composition. The MD technique uses the mean vectors of each endmember and calculates the Euclidean distance from each unknown pixel to the mean vector for each class. This method made it possible to look at the mineralogical composition in detail as well as to estimate the surface percentage that each mineral covers in each sample.

Both, μ -XRF and SEM are semi-quantitative methods. To accurately determine the chemical composition of plagioclase feldspars, two to four plagioclase crystals per thin section were further analyzed using an EPMA. An electron beam coming from the microprobe, a *CAMECA SX1000* from Georesources, Nancy (France), bombards the samples. In response, X-rays are emitted by the sample at the characteristic wavelength for each element. The EPMA employs a similar technique as SEM with standards of each element being used to quantify their content in the analyzed crystals. To determine the chemical composition of feldspars in the samples, the elements analyzed are Na, Ca, K, Al, Si, O, and Fe.

2.2. Reflectance Spectroscopy

VNIR reflectance spectroscopy (0.4–4 μm) is a widely used technique in planetary science to detect minerals remotely (e.g., Clark et al., 2003).

Reflectance spectroscopy measurements were carried out on macroscopic samples using an *ASD Fieldspec 4* point-spectrometer. The instrument combines three different detectors in the VNIR (0.350–1.000 μm), SWIR 1 (1.001–1.800 μm), and SWIR 2 (1.801–2.500 μm) to make a spectrum in the full 0.35–2.50 μm range. Spectral resolution varies with the VNIR and SWIR detectors having 3 and 8 nm resolutions, respectively. Spectra were collected with the instrument contact probe and calibrated with reference panels of 10% or 50% reflectance

depending on the darkness level of each sample. The contact probe views a circular area of approximately 2 cm in diameter, leading to the acquisition of a spectrum representative of all grains contributing within the viewing area, and then to the rock itself. These total rock spectra acquired are comparable to those of remote sensing hyperspectral measurements.

In order to show the scope of the study of whole rocks in comparison with previous studies interested in powders or grains (Adams & Goullaud, 1978; Cheek & Pieters, 2014; Crown & Pieters, 1987; Rogers & Nekvasil, 2015), we chose to also study the powders of our five samples, NJ2, NJ11, NM6, NR1 and NR2, with the *ASD Fieldspec 4* point-spectrometer, and more precisely with its accessory, the Mug-Light (2 cm diameter spot). The samples were first crushed with a jaw crusher and then porphyzied with an agate vibratory disc mill. The grain size of the powders is then <80 μm .

All these spectra acquired with the *ASD Fieldspec 4* on both rocks and powders were then normalized using the Continuum Removal process available in ENVI. This continuum is a convex hull that fits the spectrum using straight-line segments that connect local maxima. The first and last reflectance values are equal to 1.

We further used hyperspectral cameras to resolve finer spatial scales and acquire spectra of each mineral contained in these rocks. As opposed to the one-dimensional data of *ASD Fieldspec 4* point-spectrometer (spectra), data from hyperspectral cameras are three dimensional, consisting of a two-dimensional image plus the spectral data as the third dimension (hyperspectral cubes). We acquired hyperspectral images of the samples with the HySpex *VNIR-3000-N* and *SWIR-640* cameras that operate from 0.40 to 1.00 μm and from 0.96 to 2.50 μm , respectively. At a distance of 30 cm from the sample, the resulting pixel size is about 39 and 130 μm in the VNIR and SWIR, respectively. The hyperspectral cubes are converted to reflectance using reference panels of 10% or 50% reflectance depending on the darkness level of each sample. The analyses of the cubes were performed with the ENVI image processing software to classify the image pixels according to their spectral signature. We used the Spectral Angle Mapper (SAM) method, which is one of the supervised classification methods available in ENVI (Kruse et al., 1993); this algorithm determines the spectral similarity between two spectra by calculating the angle between the spectra of the hyperspectral cube and a given reference spectrum (known as an “endmember”). Endmembers were handpicked to map as many mineral classes as expected from the petrographic analyses of the samples. This classification then provides mineralogical maps and associated statistics that give the mineral surface abundances according to the class created with SAM based on the endmembers.

Both the total rock spectra or powder spectra acquired with the *ASD Fieldspec 4*, and the spectra of minerals acquired with hyperspectral cameras were then compared to the USGS reference spectral library (Kokaly et al., 2017) to identify mineral signatures.

The plagioclase absorption band, observed in the spectra of total rocks, powders, and plagioclases in each sample themselves, is located in the 0.8–1.7 μm region. The plagioclase band centers were then determined numerically with a custom-made python routine. First, the slight gaps in spectra arising from the three separate detectors (in the case of *ASD Fieldspec 4* spectra) were realigned in order to avoid interpreting them as real spectral features. Next, plots of spectra were visually inspected for narrow bands that typically arise from the hydration of minerals or other bands due to associated minerals present in the rock (e.g., olivine). If narrow bands were found, the portion of the spectra where these bands overprint the broad band of plagioclase was removed and reconstructed using spline interpolation (linear, quadratic, or cubic), second-degree polynomial fitting, or third-degree polynomial fitting, chosen through trial and error. Then, to reduce high-frequency, low-amplitude noise, spectra were smoothed using a Savitzky-Golay filtering method with a third order polynomial and a window size ranging 51–81 wavelengths. Finally, the minimum was sought in a chosen wavelength range according to each spectrum (on average between 0.9 and 1.5 μm): this minimum gives the plagioclase band center position.

3. Results

3.1. Mineralogical and Elemental Composition

The mineralogical composition of each sample was first assessed by optical microscopy. Results are described in Table 1g and representative pictures of the thin sections of each sample observed in transmitted light are shown in Figure S1 (Supporting Information S1). All samples contain plagioclase feldspar as well as a diversity of associated minerals depending on the rock composition (e.g., olivine and/or pyroxene for mafic rocks and

Table 1
Summary Table of Data Obtained From Analyses and Processing of the Five Terrestrial Feldspar-Bearing Rock Samples (NJ2, NJ11, NM6, NR1, and NR2)

Analysis type	a.	b.	c.	d.	e.	f.	g.
	Plagioclase surface abundance (SEM)	Plagioclase surface abundance (Hyperspectral cubes)	Anorthite in plagioclases (EPMA)	FeO in plagioclases (EPMA)	Band center wavelength of total rock spectrum (Fieldspec)	Plagioclase band center wavelength (Hyperspectral cubes)	Mineralogical composition (Optical microscopy)
N-J-2 Dacite	20.40%	53.92%	40.90 mol%	0.21 w%	1.16 μm	1.16 μm	Plagioclase phenocrysts, biotite, amphibole and potassic feldspar—Small crystals of oxide—Plagioclase microlites—Porosity
N-J-11 Granite	17.55%	47.61%	25.00 mol%	0.18 w%	1.16 μm	1.22 μm	Altered plagioclase, potassic feldspar (orthoclase), biotite (sometimes altered in chlorite), calcite
N-M-6 Anorthosite	88.83%	81.25%	53.63 mol%	0.25 w%	1.45 μm	1.42 μm	Almost exclusively composed of plagioclase, altered pyroxene, and epidote
N-R-1 Basalt	69.98%	54.08%	67.17 mol%	0.73 w%	1.19 μm	1.29 μm	Phenocrysts and microlites of plagioclase and altered olivine (iddingsite)—Small crystals of oxide
N-R-2 Basalt	9.74%	32.15%	54.54 mol%	0.69 w%	1.38 μm	1.22 μm	Plagioclase and olivine (altered or not) phenocrysts—Small crystals of clinopyroxene—Plagioclase and olivine microlites—Volcanic glass surrounding plagioclase phenocrysts

Note. a. Plagioclase surface abundance determined by Minimum Distance (MD) classification (ENVI, L3Harris Geospatial) made from the Scanning Electron Microscope (SEM) false-color chemical maps R = Ca; G = Na; B = K. b. Average surface abundance of plagioclase determined by SAM classification made with the VNIR and SWIR data cubes acquired with hyperspectral cameras. c. Anorthite average content in plagioclases determined with Electron Probe MicroAnalyzer (EPMA). d. FeO average content in plagioclases determined with Electron Probe MicroAnalyzer (EPMA). e. Position of the plagioclase absorption band center on the total rock spectrum acquired with the ASD *Fieldspec 4* and determine using our Python code (Figure S13 in Supporting Information S1). f. Position of the plagioclase absorption band center (Figure S15 in Supporting Information S1) on the plagioclase class spectrum determined by SAM classification based on the SWIR hyperspectral data cube. g. Mineralogical composition as inferred from optical microscopy.

biotite and K-feldspar for more felsic rocks). Chemical maps of the thin sections acquired with the SEM confirm the mineralogical composition determined by optical microscopy. In addition, SEM (Table 1a and Figure 2) and μ -XRF (Figure S7 in Supporting Information S1) analyses provided first estimates of the composition of feldspars and their abundance.

Optical microscopy observation located feldspar crystals on the thin sections of the samples, and the SEM data provide further information that enables the characterization of the potassic, alkali or plagioclase nature of feldspars. All the samples contain plagioclase with varying compositions between the sodic and the calcic endmembers (Figure 2). In addition to plagioclase, NJ11 (granite) contains potassic feldspars and NR2 (basalt) contains alkali feldspars. The percentage of plagioclase contained in each thin section was then determined using a Low Pass filter to smooth the noisy SEM data prior to MD classification (Figure S2 in Supporting Information S1). Plagioclase, of various compositions, represent between $\sim 9\%$ and $\sim 88\%$ of the samples, however, classifications on the SEM maps do not always capture the microcrystals contained in the groundmass of samples NJ2 (dacite) and NR2 (basalt) because of the noise contained in the data. The granite NJ11 contains partially altered plagioclase crystals, which are not taken into account in the total amount of plagioclase. Hence, the plagioclase content determined with the SEM data of these three samples is likely underestimate of the total amount of plagioclase feldspars. Similar petrographic observations were made from μ -XRF data, which are even less resolved than SEM data, and are presented in Figure S7 (Supporting Information S1).

Following these analyses, measurements with the EPMA were performed in order to obtain quantitative compositions. The location of the EPMA analysis points is shown in Figure 2 on the SEM chemical maps. Several feldspars of different sizes, both plagioclase and alkaline, were measured in each sample. The results obtained are plotted in Figure 3a according to their calcium, sodium, and potassium content in the classical feldspar ternary diagram. The diversity of our samples makes it possible to cover a wide range of feldspar compositions.

In order to accurately determine the chemical composition of plagioclase crystals, the anorthite (An) content was determined based on the known chemical formula of the two plagioclase endmembers: sodic plagioclase ($\text{NaAl-Si}_3\text{O}_8$) and calcic plagioclase ($\text{CaAl}_2\text{Si}_2\text{O}_8$). Iron is not part of the theoretical composition of plagioclase but can be incorporated in small quantities through elemental substitution (Adams & Goulaud, 1978), as discussed in Section 4.2.

Table 1c and 1d show the average An and Fe contents in analyzed plagioclase crystals for each sample. Values are the average An and Fe contents of all plagioclase crystals measured in each sample (Figures S8–S12 and Table S1 in Supporting Information S1). Plagioclase crystals in basalt NR1 have the highest An and Fe contents of all samples, with An_{67} and 0.73 wt% FeO. Plagioclase crystals in NJ11 granite, on the other hand, contain only An_{25} and 0.18 wt% FeO. As Figure 3b shows, plagioclase An and Fe contents are positively correlated.

3.2. VNIR Spectral Signature

The macroscopic samples and their corresponding powders were spectrally characterized in the VNIR with the *ASD Fieldspec 4* instrument. Figure 4a shows the rock spectra (solid lines) and powder spectra (dotted lines) of the five samples NJ2, NJ11, NM6, NR1, and NR2, as well as a reference spectrum of anorthite powder from the USGS Spectral Library (Kokaly et al., 2017). Figure 4b shows the same spectra with the continuum removed using the convex hull method available in the ENVI software. In both Figures 4a and 4b, spectra are plotted with an offset for clarity.

All macroscopic samples show a broad absorption band centered around 1.3 μm . This band center varies from one sample to another: 1.16 for NJ2 (dacite) and NJ11 (granite), 1.19 for NR1 (basalt), 1.38 for NR2 (basalt), and 1.45 μm for NM6 (anorthosite). These values are reported in Table 1e and in Figure S13 (Supporting Information S1).

Powders of the same samples with a particle size of less than 80 μm were also analyzed using the *ASD Fieldspec 4*. Comparison of reflectance spectra of macroscopic and powdered samples demonstrates that the shape of the spectra is clearly different even though the material composition is the same (Figure 4). When the samples contain hydrated minerals, the characteristic absorption bands of -OH compounds and H_2O at 1.4 and 1.9 μm are found in both powder and rock spectra (e.g., NJ2). The comparison of the ~ 1.3 μm absorption bands related to the electronic transitions of Fe^{2+} , however, indicates that powder and rock spectra do not have the same band center (NR1 and NR2), nor even the same shape (NJ2, NJ11, NR1, NR2) or intensity. The diagnostic feldspar

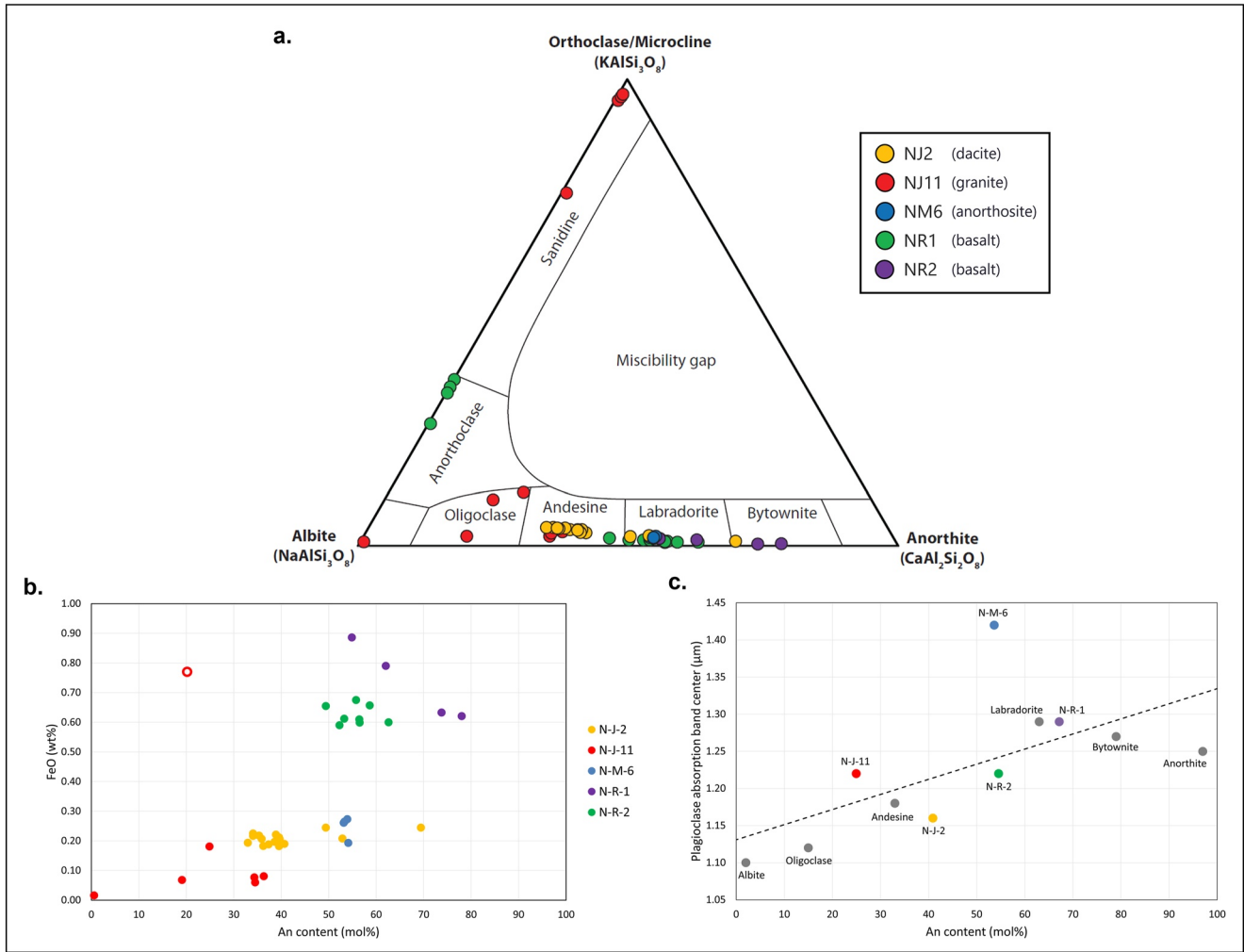


Figure 3. Results of point analyses (location of the analysis points in Figure 2) made with the Electron Probe MicroAnalyzer on thin sections of the five feldspar-bearing macroscopic samples NJ2, NJ11, NM6, NR1, and NR2. Between two and six feldspar crystals (porphyritic and microlitic) were analyzed per sample. (a) Feldspar ternary diagram showing the chemical composition of feldspar crystals. (b) FeO content as a function of An content of plagioclase feldspars of the macroscopic samples (analysis points located between Albite and Anorthite endmembers in panel (a)). As argued in Section 4.2.1, the analysis point of NJ11 indicated by an empty red circle is discarded from further discussions. (c) Plagioclase absorption band center position determined by analysis of visible near-infrared and SWIR hyperspectral data cubes as a function of An content of plagioclase feldspars of the macroscopic samples. The gray data points were extracted from Adams and Goulaud (1978).

absorption band is not visible on the powder spectra of samples NJ2 (dacite) and NJ11 (granite). The exception is the NM6 (anorthosite) sample, which is an anorthosite and contains between 80% and 90% of plagioclase feldspars (Table 1a and 1b). Both the powder and the total rock spectra of NM6 display the diagnostic plagioclase absorption band. It should be noted that the band depth is generally lower on the powder spectra than that of the macroscopic samples (Figure 4).

Grain to grain analyses were performed using the VNIR-3000-N and SWIR-640 hyperspectral cameras. The mineral locations and types are known from optical microscopy and SEM data (Figure 2 and Figures S8–S12 in Supporting Information S1). The average spectrum of each mineral contained in each mineral group from each sample was obtained using a SAM classification from the ENVI software. This classification allows the determination of the percentage of each class and therefore the surface abundance of each mineral (Table 1b). Figure 5 shows the results obtained using the NR1 (basalt) sample as an example, while results for the other samples are shown in Figures S3–S6 (Supporting Information S1). The processing of SWIR data suggests that ~66% of the NR1 sample contains plagioclase (both crystals and microcrystals), while the VNIR data estimate gives us ~42%. The average spectrum of the plagioclase class in the SWIR range displays an absorption band centered at 1.29 μm, consistent with USGS

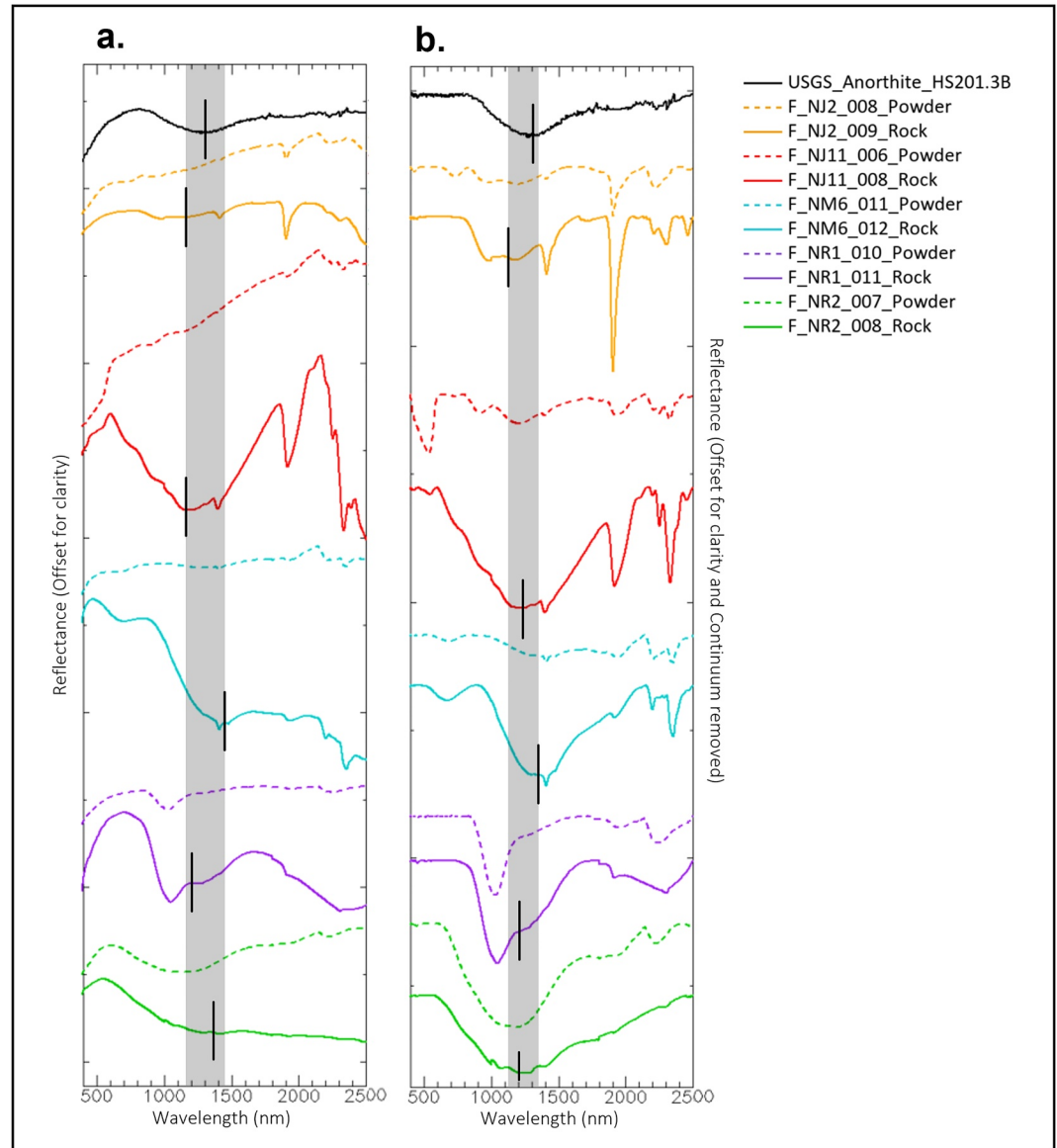


Figure 4. Reflectance spectrum of the five feldspar-bearing samples, (a) before and (b) after continuum removal. The data were acquired with the *ASD Fieldspec 4* on samples NJ2 (dacite), NJ11 (granite), NM6 (anorthosite), NR1 (basalt), and NR2 (basalt) both as powders (dotted lines) and macroscopic samples (solid lines). The black spectrum is the USGS Anorthite HS201.3B given for reference. The black vertical lines indicate the position of the center of the $\sim 1.3 \mu\text{m}$ absorption band, which can be seen in more detail in Figures S13, S14, and S16 (Supporting Information S1).

library anorthite spectrum (Figure 4) and not observed in other mineral groups from this sample. Similarly, representative spectra of each mineral present in each rock sample were extracted from the VNIR and SWIR spectral images. The spectrum of plagioclase is therefore known for each sample, and the plagioclase absorption band center position was determined using our Python code (Table 1f and Figure S3–S6 in Supporting Information S1). These values can then be compared with the ones obtained on the total rock spectra acquired with the *ASD Fieldspec 4* (Table 1e).

4. Discussion

4.1. Identification of Plagioclase VNIR Spectral Signature

For each sample, the mineralogical composition (Table 1g) and spectral signature of each mineral (e.g., NR1 sample in Figure 5) were determined. We observed that only plagioclase has an absorption band centered around

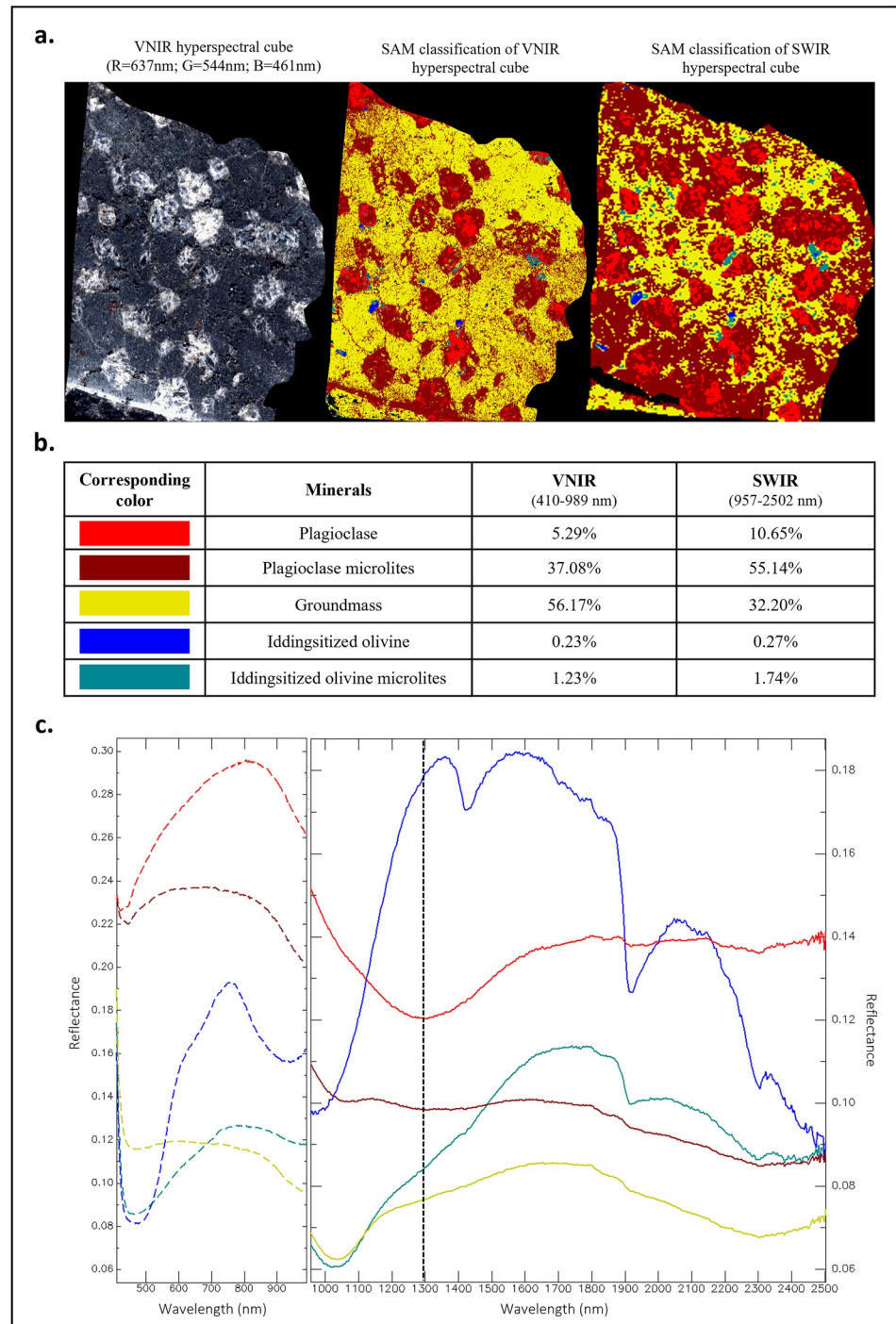


Figure 5. Visible-near-infrared (VNIR) and SWIR cube processing of the NR1 (basalt) macroscopic sample is shown as an example. The mineralogical composition of this sample is known from microscopic analyses (Table 1g), allowing us to select the spectrum of each mineral on the hyperspectral cubes and use them as endmembers. (a) Left to right: RGB composite of the VNIR hyperspectral cube (true colors); result of the Spectral Angle Mapper (SAM) classification made with ENVI on the VNIR hyperspectral cube; result of the SAM classification made with ENVI on the SWIR hyperspectral cube. (b) Table showing which mineral class the SAM classification colors correspond to and the surface abundance of each mineral class in the VNIR and SWIR domains. (c) Reflectance spectrum of each mineral class after SAM classification in the VNIR and SWIR domains. The graphs were placed side by side to observe continuity between domains, although a gap in absolute reflectance might be observed between the two different instruments. The wavelength units chosen for this graph are nanometers.

1.3 μm with broad shoulders at 0.8 and 1.7 μm . The same absorption band is observed on the total rock spectra of all studied macroscopic samples and on the USGS anorthite spectrum (Figure 4, Kokaly et al., 2017). We therefore conclude that this absorption is the spectral signature of plagioclase feldspar. It should, however, be noted that in the groundmass of volcanic samples, which is composed of plagioclase and mafic minerals (such as olivine, pyroxene, biotite, or amphibole), this band is no longer visible (Figure 5c). Both the presence of mafic minerals and the smaller crystal sizes could explain why plagioclase absorption band vanished in the groundmass. Mafic minerals are indeed known to mask the spectral signature of plagioclase by overlaying or attenuating its absorption band (e.g., Cheek & Pieters, 2014).

In the spectra of the macroscopic samples acquired with the *ASD Fieldspec 4* (Figure 4), the position of the plagioclase-related absorption band seems to vary. This band center varies from one sample to another: it is observed around 1.16 for NJ2 (dacite) and NJ11 (granite), 1.19 for NR1 (basalt), 1.38 for NR2 (basalt), and 1.45 μm for NM6 (anorthosite). These values are not always consistent with the results obtained using the hyperspectral cameras (Table 1f). For instance, the average spectrum of the plagioclase mineral group in basalt NR1 (measured with the hyperspectral cameras) has an absorption band centered at 1.29 μm while the spectrum of the macroscopic sample (measured with the *ASD Fieldspec 4*) has an absorption band centered at 1.19 μm . Basalt NR1 also contains olivine crystals which have a broad absorption centered around 1 μm , which likely contribute to the total rock spectrum. Hence, the observed absorption in the total rock spectrum is likely a combination of both the olivine and plagioclase signatures. The shape of the absorption band can indeed be related to the plagioclase chemical composition but also to the grain size: the larger the size of the grains, the deeper the plagioclase absorption band.

The presence of other minerals may contribute to the total spectrum of the rock in both its macroscopic and crushed state, as confirmed by the analysis of the spectra of powders NR1 and NR2 (basalts), which both have an absorption band related to the presence of olivine centered around 1 μm . On these powder spectra, only the olivine spectral signature at 1 μm is visible, whereas these crushed rocks contain $\sim 43\%$ of plagioclase according to the hyperspectral data (Table 1b). The ambiguity due to the presence of an olivine absorption band on the powder spectra led us to work with whole, uncrushed rocks as a better analog to Mars remote sensing data.

Other minerals in spectral libraries can display absorption features at similar wavelengths than plagioclase, such as biotite, pyroxene, muscovite, chlorite, glass, or almandine garnet (e.g., Henderson et al., 2020; Horgan et al., 2014; Scudder et al., 2021; Wray et al., 2013). Biotite is part of the mineral assemblage that makes up NJ2 (dacite) and NJ11 (granite) samples, plotted in yellow (NJ2) and red (NJ11), respectively, in Figure 4, whereas chlorite and muscovite are common alteration products of biotite and plagioclase respectively. The 1.2 μm absorption band of biotite, unlike plagioclase, does not have a left shoulder in the visible range. This observation is confirmed by the average spectrum of biotite obtained after processing hyperspectral VNIR and SWIR images. Biotite also has a diagnostic doublet absorption at 2.33 and 2.40 μm that helps to discriminate it from other minerals, while chlorite and muscovite present diagnostic absorptions at 2.32/2.39 μm and 2.35/2.44 μm respectively. Chlorite, muscovite, biotite, and other plagioclase alteration products, also have a broad absorption band centered around 1.2 μm in addition to typical H_2O and $-\text{OH}$ absorptions around 1.4 and 1.9 μm . Therefore, we cannot exclude that the biotite, muscovite, and chlorite signatures add up to the plagioclase absorption band feature to make the final band observed in the total rock spectrum. What should be noted here is that plagioclase contributes to the presence of an absorption band around 1.3 μm on the total rock spectrum of all samples.

Our study, therefore, shows that it is indeed possible to detect the presence of plagioclase feldspar in a magmatic rock, even though it does not contain 90% feldspar, and regardless of its nature (e.g., effusive rock NR1 shown in Table 1b contains $\sim 54\%$ of plagioclase according to hyperspectral data).

Both VNIR and SWIR hyperspectral cubes were used to provide estimates of surface percentages from the classification statistics (Figure 5b, Table 1b, Figures S3–S6 in Supporting Information S1), with discrepancies between the VNIR and the SWIR cubes. We argue that these differences could have two distinct origins: (a) the VNIR cube has a resolution twice that of the SWIR cube. The pixel size in the SWIR is sometimes too large for the classification to efficiently distinguish the groundmass from the plagioclase microlites; and (b) in the VNIR range, the plagioclase crystals and microlites spectra are too similar for the classification to distinguish the plagioclase crystals from the plagioclase microlites. Thus, in the example of the NR1 sample (Figure 5), the obtained percentage is between $\sim 42\%$, obtained in the VNIR, and $\sim 66\%$, obtained in the SWIR.

The amount of plagioclase was estimated based on hyperspectral camera data but also on SEM chemical maps. Comparing the results of the two methods for samples NJ2 (dacite), NJ11 (granite), and NR2 (basalt) in Table 1a and 1b, large differences in values are observed. NJ11, taken as an example, the SEM data give 17.55% plagioclase while hyperspectral camera data give 47.61%. In NJ11 and NR2, some plagioclase crystals are altered: altered and fresh plagioclases are similarly classed from hyperspectral camera data, while altered and fresh plagioclases are differentiated in SEM chemical maps. Another source for discrepancies is the texture of samples NJ2 and NR2, which are volcanic rocks with plagioclase microlites in the groundmass. The plagioclase microlites are not considered in the total percentage of plagioclase contained in NJ2 and NR2 based on the noisy SEM data, unlike the classification made based on hyperspectral data.

4.2. Influence of Plagioclase Composition

4.2.1. Correlation Between the Fe and An Contents

Pure feldspars are considered to have no absorption band in the VNIR and SWIR ranges. However, plagioclase feldspars can incorporate a small amount of Fe^{2+} in their structure. An absorption band centered around $1.25 \mu\text{m}$ is then visible on their reflectance spectrum (Adams & Goullaud, 1978): the greater the amount of Fe^{2+} incorporated, the deeper the absorption band at $1.25 \mu\text{m}$ (Bell & Mao, 1973).

The incorporated ferrous iron can occupy M-sites by replacing Ca^{2+} (Appleman et al., 1971; Hafner et al., 1971; Hofmeister & Rossman, 1984). About 90% of the time, however, Fe^{2+} occupies T-sites with a double substitution of $\text{Fe}^{2+} + \text{Si}^{4+} \rightleftharpoons 2\text{Al}^{3+}$ (Adams & Goullaud, 1978; Longhi et al., 1976; Lundgaard & Tegner, 2004). In both cases, the plagioclase feldspar will have an absorption band $\sim 1.25 \mu\text{m}$ on its reflectance spectrum, although occupation of the T-sites will result in an absorption band twice as deep as when Fe^{2+} occupies M-sites sites (Burns, 1993). Only plagioclase feldspars can incorporate Fe^{2+} since they are the only feldspars composed of Ca^{2+} and 2Al^{2+} (Smith & Brown, 1988). Alkali feldspars, on the other hand, do not have the necessary chemical composition to host Fe^{2+} although they may sometimes contain plagioclase impurities and thus exhibit a $\sim 1.25 \mu\text{m}$ absorption band.

The chemical analyses carried out on the five terrestrial feldspar-bearing rock samples with the EPMA were therefore performed in order to determine the composition of feldspars, potassic and plagioclase, of microlithic and porphyritic size. The results are gathered in a feldspar diagram (Figure 3a). The crystal chemical compositions in the five samples cover a wide range of possible plagioclase feldspar types.

To understand the influence of plagioclase composition on their spectral signature, we compare the An content with the Fe content (Figure 3b), and the An content with the position of the plagioclase absorption band obtained with the classification on hyperspectral cubes (Figure 3c). A positive correlation between the content of An and Fe is observed. This relationship could be related to the evolution of the magma composition during its crystallization as observed in various cases (e.g., Bowen, 1928; Couturié, 1977; De Wit & Kruger, 1990; Irvine, 1970). Ca-rich plagioclase and iron oxides are therefore expected to be among the first minerals to form in magmas. Over fractional crystallization, most magmas become gradually depleted in calcium and iron, and, hence, plagioclase becomes less and less calcic. This is in line with our EPMA analyses that show that the cores of plagioclase crystals are richer in An than the margins, suggesting that the amount of Ca decreased in the magma as it cooled down and crystallized. Alternatively, the redox state of the magma, which also evolves during crystallization, could possibly explain why more sodic plagioclase contain less iron, assuming that the iron is in the Fe^{3+} state in more evolved melts. Among the unknowns, there is the possible effect of crystallization speed and cooling rates on the incorporation of iron into plagioclases.

Our results show a clear correlation between An and Fe content, in spite of Lundgaard and Tegner (2004) results that suggest that Fe content is independent of plagioclase composition. In addition to the availability of the different elements in the magma during its crystallization, the initial composition of the magma, its redox state and the cooling rate are among the many factors that could play a role in the incorporation of Fe^{2+} in feldspars.

Our data are well-correlated except for one of the data points in NJ11 (granite), which contains 0.88 wt% FeO (Figure 3b); hence, it is seven times richer in iron than the other crystals studied. This measurement was made on the edge of a plagioclase crystal, close to a mafic mineral, which likely biased the final result. This hypothesis is supported by the fact that the center of this plagioclase crystal was also analyzed and gave an iron content of

0.08 wt% despite similar An content. The 0.88 wt% FeO point in NJ11 will therefore not be taken into consideration in the following discussion.

The overall trend in the data (Figure 3b) therefore indicates a positive correlation between the An and FeO content. Within the same sample, however, this trend is not always observed, like in the NR1 (basalt) sample. In our samples, we observe that the microcrystals contained in the groundmass contain less An than the large crystals but more iron. Within a sample, as NR1, the observed trend is then inverse to that of the entire collection.

4.2.2. Correlation Between the Band Center Position and the An Content

Figure 3c shows a correlation between the An content and the position of the plagioclase absorption band at $\sim 1.3 \mu\text{m}$: the more An in plagioclase, the more shifted to longer wavelengths the center of the absorption band. The trend therefore seems to indicate a correlation between An content and the position of the absorption band, with the exception of labradorite. Indeed, plagioclase crystals contained in NR1 (basalt) are richer in An, with 67.17%An, than NM6 (anorthosite), with 53.63%An; yet, the former has an absorption band centered at 1.29 μm and the latter at 1.42 μm (Table 1c and 1f). The same result was observed by Adams and Goullaud (1978), which showed that labradorite has an absorption band around 1.3 μm while anorthosite, which is richer in An, has an absorption band around 1.25 μm (Figure 3c).

Potassic feldspars in samples NJ11 (granite) and NR2 (basalt) also contain iron: 0.02 and 1.46 wt% on average, respectively (Table S1 and Figure S9 in Supporting Information S1). The structural formula of potassic feldspars has only one Al^{3+} . The mechanism of double substitution to incorporate Fe^{2+} (Smith & Brown, 1988) is therefore not possible for these minerals. These amounts of iron therefore correspond to the incorporation of Fe^{3+} by feldspar. The presence of Fe^{3+} in the structure of a mineral results in the presence of a characteristic band at $\sim 0.86 \mu\text{m}$, due to the absorption of blue light by the mineral, giving the red color (Adams & Goullaud, 1978).

NJ11 sample contains sanidine feldspar based on EPMA analyses. The presence of orthoclase is visible in the VNIR hyperspectral data since the reflectance spectrum of potassic feldspar has an absorption band at 0.90 μm (Figure S4 in Supporting Information S1). It should be noted, however, that iron is present in small quantities in NJ11 K-feldspar crystals compared to NR2. However, the reflectance spectrum in the VNIR of the anorthoclase contained in NR2 does not show an absorption band around 0.86 μm potentially masked by the spectral signature of mafic minerals (Figure S6 in Supporting Information S1).

Although we have analyzed an average of four crystals per sample, which allows us to obtain 40 data points, in order to confirm the trends identified by our EPMA analyses, it is necessary to study a wider range of samples. This would ultimately allow us to assess the amount of Fe necessary to observe such absorptions, the influence of associated minerals, and to better understand the actual relationship between the position of the feldspar absorption band and its An and Fe contents.

4.3. Implications for Mars

Remote sensing, meteorite and in situ data consistently indicate that the surface of Mars is mostly basaltic in composition (e.g., McSween et al., 2003). However, according to recent geophysical models (Baratoux et al., 2014), large volumes of anorthositic or felsic rocks, less dense than the surficial basalt, may be buried under the southern highlands of Mars. This lower crust could be the source of some of the more exotic compositions recently detected from orbit (e.g., the anorthosites of Carter and Poulet (2013)), or observed in situ in Gale Crater by the Curiosity rover (e.g., the granodiorites of Sautter et al. (2016)), although fractional crystallization and other magmatic processes can also explain the occurrence of more alkaline and/or evolved, trachytic (Sautter et al., 2015) and dacitic (Christensen et al., 2005) compositions, locally.

The total rock spectra, obtained using the *ASD Fieldspec 4*, are comparable to the data obtained using hyperspectral sensors onboard Martian satellites. Indeed, recent detections of plagioclase feldspars (Carter & Poulet, 2013; Farrand et al., 2021; Flahaut et al., 2022; Payré et al., 2022; Phillips et al., 2022; Rogers & Farrand, 2022; Wray et al., 2013) were made using remote sensing instruments observing the surface of Mars. The interpretation of these signatures, in terms of lithologies is still under discussion given the variety of geological contexts presented in several studies (Carter & Poulet, 2013; Farrand et al., 2021; Flahaut et al., 2022; Payré et al., 2022; Phillips et al., 2022; Rogers & Farrand, 2022; Wray et al., 2013).

Our study further shows that a number of rock types can carry plagioclase signatures, leading to many possible interpretations. Detections of plagioclase on the surface of Mars could be consistent with primitive anorthositic

rocks (Carter & Poulet, 2013; Phillips et al., 2022), as well as secondary volcanic rocks (Farrand et al., 2021; Flahaut et al., 2022; Payré et al., 2022; Rogers & Farrand, 2022), or even felsic tertiary rocks (Sautter et al., 2015), given that all of our anorthosite, basalt, dacite and granite rock samples show similar signatures. The construction of a reference library acquired on macroscopic rock fragments that we undertook should lead to a more accurate interpretation of Martian detections.

4.4. Limits and Perspectives

The chemical composition of plagioclase feldspars, grain size, and associated minerals play a major role in the VNIR spectral signature of the macroscopic rocks. Our study shows that the signature of plagioclase is visible on all the total rock spectra but not systematically on the spectra of powders. Rocks containing only few mafic minerals, such as NM6 (anorthosite), which contains between 5% and 10%, display a plagioclase absorption band on their powder spectrum only slightly affected by the signature of mafic minerals. As shown in the study of Cheek and Pieters (2014), the four other samples have their powder spectrum dominated by the mafic mineral spectral signatures, which overlay or attenuate the plagioclase absorption band.

Whether samples are studied as a macroscopic rock or as powder will cause variations in its VNIR spectral signature. The grain size has indeed been shown to strongly influence the spectral signature, including its presence, shape, width, and intensity (Clark et al., 2003). The study of macroscopic samples and not powders in the laboratory therefore seems to be more accurate for the study of rocks on the surface of planets by remote sensing.

As discussed in Section 4.1, associated minerals can also contribute to the average spectrum of the macroscopic sample and modify the resulting plagioclase absorption band center and shape. It would be interesting to study the asymmetry and width of the absorption band around 1.3 μm to determine potential overprints from biotite and olivine minerals, among others.

The surface alteration of samples and natural roughness were not accounted for in our study; however, these factors are known to influence the spectral signatures of rocks. All of our measurements were indeed carried out on fresh cut pieces of rocks, which is not an ideal match to the naturally exposed outcrops which are on Mars.

Spectral data obtained in this study can be applied to the study of feldspar-bearing igneous rocks at the surface of rocky planets as we measured directly on natural macroscopic samples, instead of pure minerals and powders. Still, it is necessary to consider the significant difference in scale between our laboratory studies, at a centimeter scale, and the resolution of remote sensing data, at a decameter scale. We made sure to analyze a representative part of our rock samples, shown in Figure 1; however, more heterogeneities in Martian outcrops could regularly exist given the spatial resolution of the instruments which are used (18 m/pixel at best for the Mars CRISM instrument).

5. Conclusions

Five feldspar-bearing macroscopic samples were analyzed using optical microscopy, SEM, EPMA and reflectance spectroscopy (point-spectrometer and hyperspectral cameras). The samples were characterized spectrally, petrographically, and geochemically in order to describe in detail the samples and try to relate their VNIR spectral signature to one of the plagioclase feldspars. The results show that the absorption band of plagioclase feldspars in the VNIR domain is visible on all five of the macroscopic samples spectra even though they contain varying amount of plagioclase (~30%–80%), but not necessarily on the corresponding powders. Analyses of mineral classes average spectra with the hyperspectral cameras confirm that the observed feature around 1.3 μm is related to plagioclase feldspar minerals, although associated minerals such as olivine or biotite tend to overlap and distort the resulting signal in the total rock spectra.

The position of this absorption band was compared with the chemical composition of the plagioclases and more precisely their iron and anorthite content. Our results suggest that there are correlations between the FeO and the An content, as well as the plagioclase absorption band center position, which generally increases with the An content (with the exception of labradorite, as already noted in previous studies). Laboratory analyses on a larger set of samples would be needed to understand those trends more accurately.

Our results demonstrate that grain size, plagioclase composition, and associated minerals must all be taken into account when interpreting VNIR spectral signatures of plagioclase; this finding contributes to the understanding of recent mineral detections made on Mars.

Data Availability Statement

Generated spectra from this study can be downloaded from the open-access Mirabelle database on the Solid Spectroscopy Hosting Architecture of Databases and Expertise (SSHADE) platform (Barthez, 2022; Flahaut et al., 2020).

Acknowledgments

Spectroscopic measurements were carried out at CRPG, Nancy (<https://crpg.univ-lorraine.fr/teledetection-hyperspectrale/>). SEM analyses were performed at CRPG, Nancy (<https://crpg.univ-lorraine.fr/microscopie-et-microsonde-electronique/>), with the help of Laurent Tissandier and Julia Neukampf. The Python code used to compile SEM maps was created by Dorian Thomassin. The authors are grateful to Jean Cauzid and Olivier Rouer from GeoRessources, Nancy, for their assistance with the μ -XRF (<http://georesources.univ-lorraine.fr/fr/content/microsonde-electronique-de-castaing>) measurements. We are very grateful to the editor Deanne Rogers for insightful comments, and to anonymous reviewer and Dr. Marie Henderson for helpful suggestions. The samples used in this study come from all over the world and belong to the CRPG collection or to CRPG researchers, such as Béatrice Luais and Emilie Thomassot. We are grateful to them and to the Terrae Genesis museum, in the French Vosges mountains (<http://terraegenesis.org/>), for the sample loans and the fruitful discussions that helped us move forward. The authors acknowledge the support of the French Agence Nationale de la Recherche (ANR), under Grant ANR-21-CE49-0003 (MARS-Spec). This is CRPG contribution number 2848. This is contribution number 607 of the ClerVolc program of the International Research Center for Disaster Sciences and Sustainable Development of the University of Clermont Auvergne.

References

- Adams, J. B., & Goulaud, L. H. (1978). Plagioclase feldspars: Visible and near infrared diffuse reflectance spectra as applied to remote sensing. In *Proceedings of the lunar and planetary science conference* (Vol. 9, pp. 2901–2909). Retrieved from <https://adsabs.harvard.edu/full/1978LPSC....9.2901A>
- Albee, A. L., Palluconi, F. D., & Arvidson, R. E. (1998). Mars global surveyor mission: Overview and Status. *Science*, 279(5357), 1671–1672. JSTOR. <https://doi.org/10.1126/science.279.5357.1671>
- Appleman, D. E., Nissen, H.-U., Stewart, D. B., Clark, J. R., Dowty, E., & Huebner, J. S. (1971). Studies of lunar plagioclases, tridymite and cristobalite. In *Proceedings of the lunar science conference*, (Vol. 1, pp. 117–133). Retrieved from <https://adsabs.harvard.edu/full/1971LPSC....2..117A>
- Baratoux, D., Samuel, H., Michaut, C., Toplis, M. J., Monnerau, M., Wiczorek, M., et al. (2014). Petrological constraints on the density of the Martian crust. *Journal of Geophysical Research: Planets*, 119(7), 1707–1727. <https://doi.org/10.1002/2014JE004642>
- Barthez, M. (2022). VNIR and SWIR spectra of terrestrial feldspathic rocks and powders (sample NR1 as an example) [Dataset]. SSHADE/Mirabelle (OSUG Data Center). [Dataset/Spectral Data]. https://doi.org/10.26302/SSHADE/EXPERIMENT_MB_20230522_0001
- Bell, P. M., & Mao, H. K. (1973). Optical and chemical analysis of iron in Luna 20 plagioclase. *Geochimica et Cosmochimica Acta*, 37(4), 755–759. [https://doi.org/10.1016/0016-7037\(73\)90172-5](https://doi.org/10.1016/0016-7037(73)90172-5)
- Bibring, J. P., Langevin, Y., Mustard, J. F., Poulet, F., Arvidson, R., Gendrin, A., et al. (2006). Global Mineralogical and Aqueous Mars History Derived from OMEGA/Mars Express Data. *Science*, 312(5772), 400–404. <https://doi.org/10.1126/science.1122659>
- Bowen, I. S. (1928). Series spectra of potassium and calcium. *Physical Review*, 31(4), 497–502. <https://doi.org/10.1103/PhysRev.31.497>
- Burns, R. G. (1993). Mineralogical applications of crystal field theory. Cambridge topics in mineral physics and chemistry (2nd ed.). Retrieved from <https://cambridge.org/9780521430777>
- Carter, J., & Poulet, F. (2013). Ancient plutonic processes on Mars inferred from the detection of possible anorthositic terrains. *Nature Geoscience*, 6(12), 1008–1012. <https://doi.org/10.1038/ngeo1995>
- Cheek, L. C., & Pieters, C. M. (2014). Reflectance spectroscopy of plagioclase-dominated mineral mixtures: Implications for characterizing lunar anorthosites remotely. *American Mineralogist*, 99(10), 1871–1892. <https://doi.org/10.2138/am-2014-4785>
- Chicarro, A., Martin, P., & Trautner, R. (2004). The Mars express mission: An overview. In A. Wilson & A. Chicarro, (Eds.). *Mars express: The scientific payload* (pp. 3–13). ESA Publications Division. Retrieved from <https://adsabs.harvard.edu/full/2004ESASP1240...3C>
- Christensen, P. R., Jakosky, B. M., Kieffer, H. H., Malin, M. C., McSween, H. Y., Neals, K., et al. (2004). The Thermal Emission Imaging System (THEMIS) for the Mars 2001 Odyssey Mission. *Space Science Reviews*, 110(1/2), 85–130. <https://doi.org/10.1023/B:SPAC.0000021008.16305.94>
- Christensen, P. R., McSween, H. Y. Jr., Bandfield, J. L., Ruff, S. W., Rogers, A. D., Hamilton, V. E., et al. (2005). Evidence for magmatic evolution and diversity on Mars from infrared observations. *Nature*, 436(7050), 504–509. <https://doi.org/10.1038/nature03639>
- Clark, R. N., Swayze, G. A., Livo, K. E., Kokaly, R. F., Sutley, S. J., Dalton, J. B., et al. (2003). Imaging spectroscopy: Earth and planetary remote sensing with the USGS Tetracorder and expert systems. *Journal of Geophysical Research*, 108(E12), 5131. <https://doi.org/10.1029/2002JE001847>
- Couturié, J. P. (1977). *Le massif granitique de la Margeride (Massif Central Français)*. Thèse de doctorat. Université de Clermont II. Retrieved from <https://hal.science/tel-01557221/>
- Crown, D. A., & Pieters, C. M. (1987). Spectral properties of plagioclase and pyroxene mixtures and the interpretation of lunar soil spectra. *Icarus*, 72(3), 492–506. [https://doi.org/10.1016/0019-1035\(87\)90047-9](https://doi.org/10.1016/0019-1035(87)90047-9)
- De Silva, S. L., Self, S., Francis, P. W., Drake, R. E., & Carlos, R. R. (1994). Effusive silicic volcanism in the Central Andes: The Chao dacite and other young lavas of the Altiplano-Puna Volcanic Complex. *Journal of Geophysical Research*, 99(B9), 17805–17825. <https://doi.org/10.1029/94JB00652>
- De Wit, M. J., & Kruger, F. J. (1990). The economic potential of the Dufek Complex. In J. F. Spletstoesser & G. A. Dreschhoff (Eds.), *Mineral resources of Antarctica* (Vol. 51, pp. 33–52). M. Antarctic Res. Ser. <https://doi.org/10.1029/AR051>
- Farrand, W. H., Rice, J. W., Jr., Chuang, F. C., & Rogers, A. D. (2021). Spectral and geological analyses of domes in western Arcadia Planitia, Mars: Evidence for intrusive alkali-rich volcanism and ice-associated surface features. *Icarus*, 357, 114111. <https://doi.org/10.1016/j.icarus.2020.114111>
- Fassett, C. I., & Head, J. W. III. (2005). Fluvial sedimentary deposits on Mars: Ancient deltas in a crater lake in the Nili Fossae region. *Geophysical Research Letters*, 32(14), L14201. <https://doi.org/10.1029/2005GL023456>
- Flahaut, J., González-Maurel, O., Godoy, B., Martinot, M., & Guitreau, M. (2021). Rheology of the Andean domes as an analog for lunar silicic constructs. In *EGU General Assembly Conference Abstracts* (pp. EGU21–11780). <https://doi.org/10.5194/egusphere-egu21-11780>
- Flahaut, J., Ito, G., Barthez, M., & Payet, V. (2020). SSHADE/Mirabelle: "CRPG" database. SSHADE (OSUG Data Center). [Database]. <https://doi.org/10.26302/SSHADE/MIRABELLE>
- Flahaut, J., Payet, V., Fueten, F., Guitreau, M., Barthez, M., Ito, G., & Allemand, P. (2022). New Detections of Feldspar-Bearing Volcanic Rocks in the Walls of Valles Marineris, Mars. *Geophysical Research Letters*, 50(2), e2022GL100772. <https://doi.org/10.1029/2022GL100772>
- Hafner, S. S., Virgo, D., & Warburton, D. (1971). Oxidation state of iron in plagioclase from lunar basalts. *Earth and Planetary Science Letters*, 12(2), 159–166. [https://doi.org/10.1016/0012-821X\(71\)90072-0](https://doi.org/10.1016/0012-821X(71)90072-0)
- Henderson, M. J. B., Horgan, B. H. N., Rowe, M. C., Wall, K. T., & Scudder, N. A. (2020). Determining the Volcanic Eruption Style of Tephra Deposits From Infrared Spectroscopy. *Earth and Space Science*, 7(2), e2019EA001013. <https://doi.org/10.1029/2019EA001013>
- Hofmeister, A. M., & Rossman, G. R. (1984). Determination of Fe³⁺ and Fe²⁺ concentrations in feldspar by optical absorption and EPR spectroscopy. *Physics and Chemistry of Minerals*, 11(5), 213–224. <https://doi.org/10.1007/BF00308136>
- Horgan, B. H. N., Cloutis, E. A., Mann, P., & Bell, J. F. III. (2014). Near-infrared spectra of ferrous mineral mixtures and methods for their identification in planetary surface spectra. *Icarus*, 234, 132–154. <https://doi.org/10.1016/j.icarus.2014.02.031>
- Irvine, T. N. (1970). Heat transfer during solidification of layered intrusions. I. Sheets and sills. *Canadian Journal of Earth Sciences*, 7(4), 1031–1061. <https://doi.org/10.1139/e70-098>

- Kokaly, R. F., Clark, R. N., Swayze, G. A., Livo, K. E., Hoefen, T. M., Pearson, N. C., et al. (2017). USGS spectral library version 7. *U.S. Geological Survey Data Series*, 1035, 61. <https://doi.org/10.3133/ds1035>
- Kruse, F. A., Lefkoff, A. B., Boardman, J. W., Heidebrecht, K. B., Shapiro, A. T., Barloon, P. J., & Goetz, A. F. H. (1993). The spectral image processing system (SIPS) – Interactive visualization and analysis of imaging spectrometer data. *Remote Sensing of Environment*, 44(2–3), 145–163. [https://doi.org/10.1016/0034-4257\(93\)90013-N](https://doi.org/10.1016/0034-4257(93)90013-N)
- Longhi, J., Walker, D., & Hays, J. F. (1976). Fe et Mg in plagioclase. In *Lunar science conference* (pp. 1281–1300). Retrieved from <https://adsabs.harvard.edu/full/1976LPSC....7.1281L>
- Lundgaard, K. L., & Tegner, C. (2004). Partitioning of ferric and ferrous iron between plagioclase and silicate melt. *Contributions to Mineralogy and Petrology*, 147(4), 470–483. <https://doi.org/10.1007/s00410-004-0568-0>
- Malin, M. C., & Edgett, K. S. (2001). Mars Global Surveyor Mars Orbiter Camera: Interplanetary Cruise through primary mission. *Journal of Geophysical Research*, 106(E10), 23429–23570. <https://doi.org/10.1029/2000JE001455>
- McSween, H. Y., Grove, T. L., & Wyatt, M. B. (2003). Constraints on the composition and petrogenesis of the Martian crust. *Journal of Geophysical Research*, 108(E12), 5135. <https://doi.org/10.1029/2003JE002175>
- Melchiorri, R., Drossart, P., Fouchet, T., Bézard, B., Forget, F., Gendrin, A., et al. (2006). A simulation of the OMEGA/Mars Express observations: Analysis of the atmospheric contribution. *Planetary and Space Science*, 54(8), 774–783. <https://doi.org/10.1016/j.pss.2006.04.014>
- Morse, S. (2015). Kiglapait intrusion, Labrador. In B. Charlier, O. Namur, R. Latypov, & C. Tegner (Eds.), *Layered intrusions*. Springer Geology. https://doi.org/10.1007/978-94-017-9652-1_13
- Murchie, S., Arvidson, R., Bedini, P., Beisser, K., Bibring, J.-P., Bishop, J., et al. (2007). Compact Reconnaissance Imaging Spectrometer for Mars (CRISM) on Mars Reconnaissance Orbiter (MRO). *Journal of Geophysical Research*, 112, E05S03. <https://doi.org/10.1029/2006JE002682>
- Neukum, G., & Jaumann, R. (2004). HRSC: The high resolution stereo camera of Mars express. In A. Wilson & A. Chicarro (Ed.), *Mars express: The scientific payload* (pp. 17–35). ESA Publications Division. Retrieved from <https://adsabs.harvard.edu/full/2004ESASP1240...17N>
- Payré, V., Salvatore, M. R., & Edwards, C. S. (2022). An Evolved Early Crust Exposed on Mars Revealed Through Spectroscopy. *Geophysical Research Letters*, 49(21), e2022GL099639. <https://doi.org/10.1029/2022GL099639>
- Phillips, M. S., Viviano, C. E., Moersch, J. E., Rogers, A. D., McSween, H. Y., & Seelos, F. P. (2022). Extensive and ancient feldspathic crust detected across north Hellas rim, Mars: Possible implications for primary crust formation (Supplementary Materials). *Geology*, 50(10), 1182–1186. <https://doi.org/10.1130/G50341.1>
- Pik, R., Deniel, C., Coulon, C., Yirgu, G., Hofmann, C., & Ayalew, D. (1998). The northwestern Ethiopian Plateau flood basalts: Classification and spatial distribution of magma types. *Journal of Volcanology and Geothermal Research*, 81(1–2), 91–111. [https://doi.org/10.1016/S0377-0273\(97\)00073-5](https://doi.org/10.1016/S0377-0273(97)00073-5)
- Rogers, A. D., & Farrand, W. H. (2022). Spectral evidence for alkaline rocks and compositional diversity among feldspathic light-toned terrains on Mars. *Icarus*, 376, 114883. <https://doi.org/10.1016/j.icarus.2022.114883>
- Rogers, A. D., & Nekvasil, H. (2015). Feldspathic rocks on Mars: Compositional constraints from infrared spectroscopy and possible formation mechanisms. *Geophysical Research Letters*, 42(8), 2619–2626. <https://doi.org/10.1002/2015GL063501>
- Saunders, R. S., Arvidson, R. E., Badhwar, G. D., Boynton, W. V., Christensen, P. R., Cucinotta, F. A., et al. (2001). 2001 Mars Odyssey Mission Summary. In C. T. Russell (Ed.), *2001 Mars Odyssey*. Springer. https://doi.org/10.1007/978-0-306-48600-5_1
- Sautter, V., Toplis, M. J., Beck, P., Mangold, N., Wiens, R., Pinet, P., et al. (2016). Magmatic complexity on early Mars as seen through a combination of orbital, in-situ and meteorite data. *Lithos*, 254–255, 36–52. <https://doi.org/10.1016/j.lithos.2016.02.023>
- Sautter, V., Toplis, M. J., Wiens, R. C., Cousin, A., Fabre, C., Gasnault, O., et al. (2015). In situ evidence for continental crust on early Mars. *Nature Geoscience*, 8, 605–609. <https://doi.org/10.1038/ngeo2474>
- Scudder, N. A., Horgan, B. H. N., Rampe, E. B., Smith, R. J., & Rutledge, A. M. (2021). The effects of magmatic evolution, crystallinity, and microtexture on the visible/near-infrared and thermal-infrared spectra of volcanic rocks. *Icarus*, 359, 114344. <https://doi.org/10.1016/j.icarus.2021.114344>
- Simmler, F. (1962). Le granite des crêtes à l'Ouest de Sainte-Marie-aux-Mines (Vosges). Étude pétrographique et minéralogique. *Bulletin du Service de la Carte Géologique d'Alsace et de Lorraine*, 15(3), 81–126. <https://doi.org/10.3406/sgeol.1962.1246>
- Smith, J. V., & Brown, W. L. (1988). Chemical properties. In *Feldspar minerals*. Springer. https://doi.org/10.1007/978-3-642-72594-4_14
- Wray, J. J., Hansen, S. T., Dufek, J., Swayze, G. A., Murchie, S. C., Seelos, F. P., et al. (2013). Prolonged magmatic activity on Mars inferred from the detection of felsic rocks. *Nature Geoscience*, 6(12), 1013–1017. <https://doi.org/10.1038/ngeo1994>
- Zuber, M. T., Smith, D. E., Solomon, S. C., Muhleman, D. O., Head, J. W., Garvin, J. B., et al. (1992). The Mars Observer laser altimeter investigation. *Journal of Geophysical Research*, 97(E5), 7781–7797. <https://doi.org/10.1029/92JE00341>
- Zurek, R. W., & Smrekar, S. E. (2007). An overview of the Mars Reconnaissance Orbiter (MRO) science mission. *Journal of Geophysical Research*, 112(E5), E05S01. <https://doi.org/10.1029/2006JE002701>